Superexchange-mediated magnetization dynamics with ultracold alkaline-earth atoms in an optical lattice*

Shaobing Zhu(朱少兵)[1,2], Jun Qian(钱军)[1], and Yuzhu Wang(王育竹)[1,†]

[1] *Key Laboratory for Quantum Optics and Center for Cold Atom Physics, Shanghai Institute of Optics and Fine Mechanics, Chinese Academy of Sciences, Shanghai* 201800, *China*

[2] *University of Chinese Academy of Sciences, Beijing* 100049, *China*

(Received 6 December 2016; revised manuscript received 24 January 2017; published online 20 February 2017)

Superexchange and inter-orbital spin-exchange interactions are key ingredients for understanding (orbital) quantum magnetism in strongly correlated systems and have been realized in ultracold atomic gases. Here we study the spin dynamics of ultracold alkaline-earth atoms in an optical lattice when the two exchange interactions coexist. In the superexchange interaction dominating regime, we find that the time-resolved spin imbalance shows a remarkable modulated oscillation, which can be attributed to the interplay between local and nonlocal quantum mechanical exchange mechanisms. Moreover, the filling of the long-lived excited atoms affects the collapse and revival of the magnetization dynamics. These observations can be realized in state-dependent optical lattices combined with the state-of-the-art advances in optical lattice clock spectroscopy.

Keywords: alkaline-earth atoms, spin dynamics, spin-exchange, superexchange

PACS: 67.85.Lm, 34.50.Cx, 75.10.Jm **DOI:** 10.1088/1674-1056/26/4/046702

1. Introduction

Ultracold atomic gases in optical lattices provide a flexible and controllable platform well isolated from the environment for quantum simulation of complex and controversial problems in condensed matter physics.[1–3] Neutral atoms allow practically perfect realizations of a variety of Hubbard models and rich quantum phases.[4–9] They are also good candidates for emulating diverse spin models,[10–12] where spin–spin interactions between atoms or molecules can be implemented and manipulated by controlled collisions on a single site,[13] on-site exchange interaction,[14,15] dipolar spin-exchange interaction,[16] or superexchange interaction in optical superlattices.[17–19] In particular, the interplay between tunneling and superexchange interaction has been experimentally observed by recording magnetization dynamics of atomic spin configurations in a two-dimensional (2D) optical lattice.[20]

In parallel with the aforementioned achievements with alkali atoms, increasing theoretical and experimental efforts have evidenced the potential of alkaline-earth atoms (AEAs) as quantum simulators of extraordinary strongly correlated systems,[21,22] owing to the emergent SU(N)-symmetric spin-exchanging collisions between the atoms in $^1S_0$ ($|g\rangle$) and $^3P_0$ ($|e\rangle$) electronic clock states, respectively.[23–25] The SU(N)-symmetric feature of the two-orbital spin-exchange interactions offer experimental access to explore the Kondo lattice model and heavy-fermion physics,[26–30] where g and e atoms represent mobile electron and localized magnetic spin, respectively.

Now a question naturally arises: how do the superexchange-mediated magnetization dynamics of the g atoms behave with doped impurities (the e atoms). It is well-known that the superexchange mechanism can work for g atoms in different spins on neighboring sites, while the inter-orbital spin-exchange interaction generally happens locally when single g and e atoms coexist in a single lattice well. In this situation, the local g/e spin-exchange interaction gives rise to spin-flip events that actually change the spin configuration of the g atoms and interrupt the superexchange process. Intuitively, one may come to the conclusion that spin-exchange interaction with the impurity atoms is negative to maintain the magnetization dynamics governed by superexchange interactions. Ultracold fermionic AEAs provide unprecedented opportunities to address the issue, and we will demonstrate the invalidity of the above statement and show an interaction-modulation feature of the magnetization dynamics. Furthermore, we will also demonstrate that the filling of the e atoms has remarkable influence in the modulated magnetization dynamics.

The paper is organized as follows. In Section 2, we introduce a Hamiltonian to describe the system, taking account of tunneling and interatomic interactions. In Section 3, we calculate the time-resolved spin dynamics of the system and present the analytic results based on perturbation method to explain the modulation feature even with the dominant superexchange interaction. Section 4 discusses the effect of the filling of e atoms on the superexchange mediated magnetization. In Sec-

*Project supported by the National Key Research and Development Program of China (Grant No. 2016YFA0301504).

†Corresponding author. E-mail: yzwang@mail.shcnc.ac.cn

© 2017 Chinese Physical Society and IOP Publishing Ltd

tion 5, we discuss the possibility of experimental observation in our setup. Finally, we present a summary of our results in Section 6. For completeness, mathematical details on the perturbation method at half and unit filling are presented in Appendices A, B, and C.

2. Theoretical Model

Let us consider an array of isolated double-well potentials created by optical superlattice as depicted in Fig. 1(a). The g and e atoms are independently trapped in state-dependent lattices. For simplicity, they are assumed to be located in the lowest band of the respective lattices, as long as the vibrational level splitting is sufficiently larger than the other relevant energy scales. In each double-well, there are only two g atoms and the number of the e atoms can be one (half-filling) or two (unit-filling) by changing the atomic population in $|^3P_0\rangle$. The lattice depth of the e atoms are very deep so that the tunneling is completely forbidden. We first study the half-filling case of the doped e atoms, that is to say, a single e atom is assumed to be fixed in the left subwell. We are interested in the spin configuration of the g atoms, and label the relevant states: the antiferromagnetic (AFM) states $|1,2\rangle$, non-magnetic state $|3\rangle$, and doubly-occupied states $|4,5\rangle$. For the situations presented here, the system is well characterized by the onsite energy U_{gg}, the tunneling rate J_g and the g/e spin-exchange interaction strength V_{ex}, representing the transitions between the states marked by the arrows in Fig. 1(a).

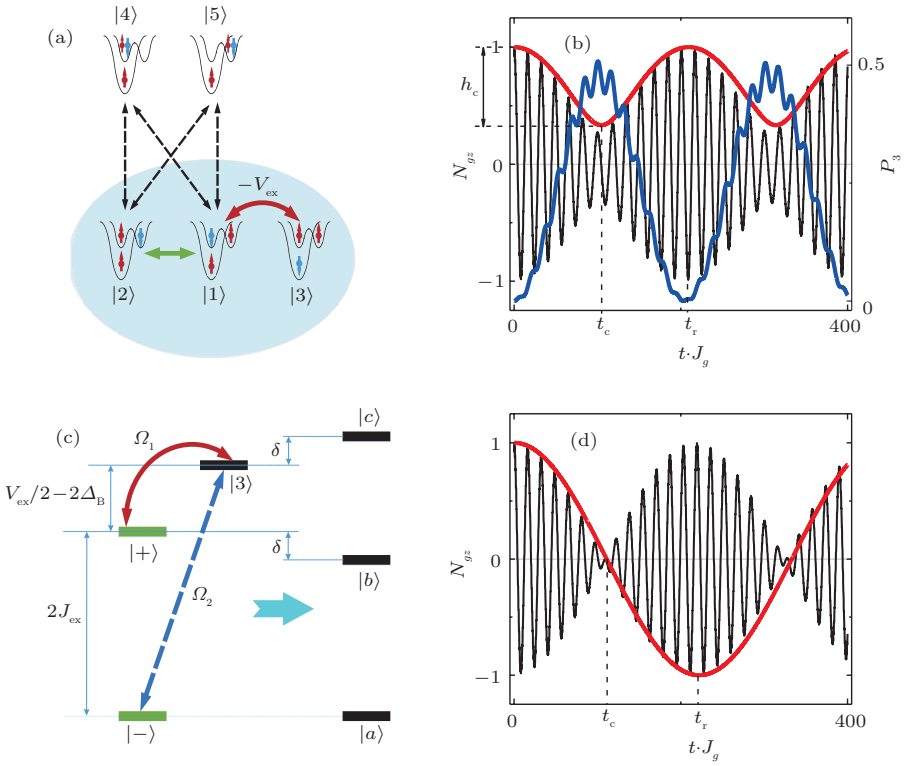


Fig. 1. (color online) (a) Schematic diagram of the superexchange and inter-orbital spin-exchange interactions. The g (e) atoms are independently trapped in the shallow (deep) superlattice, whose nuclear spin states are marked by $\uparrow$ and $\downarrow$. The superexchange process (green arrow) happens between AFM states ($|1\rangle, |2\rangle$) via virtual tunneling (black dashed arrows), while two-orbital spin-exchange interaction (red arrows) couples $|1\rangle$ with the magnetic state $|3\rangle$. (b) Time evolution of the spin imbalance N_{gz} of the g atoms (black) and the population of the state $|3\rangle$ (blue) for a small magnetic field (the resulting differential Zeeman shift can be ignored) and the initial state $|1\rangle$. The envelope of N_{gz} is given by $\sqrt{5+4\cos(3V_{\rm ex}t/2)}/3$ (red). The collapse and revival happen at $t_{\rm c}$ and $t_{\rm r}$, respectively. (c) Energy levels of the perturbation model (left) and the eigenstates (right). $|\pm\rangle = (|2\rangle \pm |1\rangle)/\sqrt{2}$. $\Omega_{1,2} = \mp V_{\rm ex}/\sqrt{2}$ are the coupling matrix elements. δ is the energy shift. The red solid and blue dashed arrows indicate the near-resonant coupling and far-off-resonant coupling, respectively. (d) Time evolution of the spin-imbalance of g atoms with $\Delta_{\rm B} = V_{\rm ex}/4$ (black line). The envelope (red solid) corresponds to $\cos(V_{\rm ex}t/\sqrt{2})$. The parameters are $U_{gg} = 10J_g$, $V = 0.025J_g$, $V_{\rm ex} = 0.02J_g$ in panels (b) and (d).

We focus on the strong-interacting regime $U_{gg} \gg J_g$, and assume that the superexchange-dominated antiferromagnetic strength predominates over the g/e spin-exchange interaction, $J_{ex} \gg V_{ex}$. The limit $U_{gg} \gg J_g$ assures that doubly-occupied states of the g atoms are allowed only via virtual tunneling and the system is antiferromagnetic ordered with the strength $J_{\rm ex} = 2J_g^2/U_{gg}$. It is well understood that, without the magnetic impurity (e atom), the system can be mapped onto a Heisenberg model with the antiferromagnetic magnetic strength $J_{\rm ex}$.[31] When the e atoms are introduced as magnetic impurities, Néel order of the g atoms may be destroyed due to the inter-orbital spin-exchange mechanism. Under these conditions the system is described by a two-site SU(N)-symmetric Fermi–Hubbard Hamiltonian as follows:

$$\hat{H} = -\sum_m J_g(\hat{c}^\dagger_{Lgm}\hat{c}_{Rgm} + \text{h.c.}) + \sum_j \frac{U_{gg}}{2}\hat{n}_{jg}(\hat{n}_{jg} - 1)$$

$$+V\sum_j \hat{n}_{je}\hat{n}_{jg}+V_{\rm ex}\sum_{j,m,m'}\hat{c}^{\dagger}_{jgm}\hat{c}^{\dagger}_{jem'}\hat{c}_{jgm'}\hat{c}_{jem}$$
$$+\sum_j \Delta_B(\hat{n}_{je\uparrow}-\hat{n}_{je\downarrow}), \quad (1)$$

where $\hat{c}^{\dagger}_{j\alpha m}$ ($\hat{c}_{j\alpha m}$) creates (destroys) an atom in state $|\alpha m\rangle$ at site $j=$L, R. The electronic and nuclear spin states are denoted by $\alpha=g,e$ and $m=\pm m_F=\uparrow,\downarrow$. $\hat{n}_{j\alpha}=\hat{c}^{\dagger}_{j\alpha m}\hat{c}_{j\alpha m}$ and $\hat{n}_{j\alpha}=\sum_m \hat{n}_{j\alpha m}$ are atomic number operators. The physics illustrated in the above equation is quite clear. The first line contains the nearest-neighbor hopping J_g between the subwells and onsite interaction of the g atoms. The second line represents the direct and spin-exchange interactions between the different electronic states.[21] In general, the influence of external magnetic field has to be taken into account, which reflects the third line in Eq. (1) in which $\Delta_{\rm B}\propto\delta gB$ is differential Zeeman shift, owing to the non-zero differential Landé g-factor δg between the clock states.[32] Mathematically,

$$U_X=\frac{4\pi\hbar^2 a_X}{M}\int {\rm d}^3 r w_a^2(\boldsymbol{r})w_b^2(\boldsymbol{r})$$

with $X=gg,ee,eg^+,eg^-$, M is the atomic mass, a_X are scattering lengths, and $w_{a,b}(\boldsymbol{r})$ are the Wannier functions of the two atoms on the same site. The associated direct and exchange interactions' strengths are $V=(U^+_{eg}+U^-_{eg})/2$ and $V_{\rm ex}=(U^+_{eg}-U^-_{eg})/2$, respectively. Constant terms have been ignored in Eq. (1). For definiteness and without loss of generality, we assume that the initial state is always $|1\rangle$ hereafter.

3. Modulated spin dynamics of superexchange interaction

We begin to study how the spin dynamics governed by the superexchange interaction is perturbed by the spin-exchange interaction in the presence of the localized e atom. In fact, the superexchange process of the two g atoms in a double-well potential can be visualized by tracing the evolution of g atom spin imbalance $N_{gz}=(\hat{n}_{Lg\uparrow}+\hat{n}_{Rg\downarrow}-\hat{n}_{Lg\downarrow}-\hat{n}_{Rg\uparrow})/2$ (Néel order parameter). We numerically calculate $N_{gz}(t)$ with the full Hamiltonian Eq. (1) and show the results in Fig. 1(b). In a clean system without the e atoms, ideally, $N_{gz}(t)$ exhibits a simple oscillation at the frequency $2J_{\rm ex}$, which has been experimentally used to extract the superexchange interaction strength.[18] It is obvious here that the superexchange-dominating magnetic dynamics features an oscillation with a modulated amplitude. The envelope of the curve is characterized by the collapse (revival) time $t_{\rm c}$ ($t_{\rm r}$) and the depth $h_{\rm c}$. One can immediately realize the fact that the spin imbalance is zero for the nonmagnetic state $|3\rangle$. $V_{\rm ex}$ results in evolving the system out of the AFM states, and consequently degrades the AFM superexchange. It should be kept in mind, however, that the spin-exchange interaction process is coherent and cannot be regarded as a pure damping mechanism for the superexchange process. It is therefore instructive to monitor the population of the nonmagnetic state $P_3(t)$. As shown in Fig. 1(b), $P_3(t)$ manifests itself as an oscillating sine-like curve. In particular, the envelope of this curve is out of phase with that of $N_{gz}(t)$. In other words, the envelope of N_{gz} approaches the minimum at $t_{\rm c}$ when the envelope of P_3 reaches the maximum simultaneously and vice versa. These results are obviously inherit to the role of inter-orbital spin-exchange interactions in the dynamics of the system.

To quantitatively understand the emergence of the modulating oscillation in the magnetization dynamics, we propose an improved perturbation strategy for revealing the behavior of the system analytically and extracting the modulation parameters. At first, similar to the superexchange process solely, the states with double occupancy ($|4\rangle$ and $|5\rangle$) are regarded as virtual intermediate states and can be adiabatically eliminated. As a result, equation (1) is reduced to the following low-energy effective Hamiltonian[31]

$$\hat{H}^{\rm eff}=2J_{\rm ex}\left(\boldsymbol{S}_{{\rm L}g}\cdot\boldsymbol{S}_{{\rm R}g}-\frac{1}{4}\hat{n}_{{\rm L}g}\hat{n}_{{\rm R}g}\right)+V\sum_j\hat{n}_{je}\hat{n}_{jg}$$
$$-2V_{\rm ex}\sum_j\left(\boldsymbol{S}_{jg}\cdot\boldsymbol{S}_{je}+\frac{1}{4}\hat{n}_{jg}\hat{n}_{je}\right)$$
$$+\sum_j\Delta_{\rm B}(\hat{n}_{je\uparrow}-\hat{n}_{je\downarrow}), \quad (2)$$

where

$$\boldsymbol{S}_{j\alpha}=\frac{1}{2}\sum\nolimits_{m,m'}\hat{c}^{\dagger}_{j\alpha m}\sigma_{mm'}\hat{c}_{j\alpha m}$$

is the local bilinear spin operators with $\sigma_{mm'}$ the Pauli matrix. Now the system governed by the effective Hamiltonian Eq. (2) has a subspace including $|1\rangle$, $|2\rangle$, and $|3\rangle$. Since $V_{\rm ex}\ll J_{\rm ex}$, the weak spin-exchange interaction has to be treated as the perturbation. Without the e atoms, the eigenstates of the effective Hamiltonian are spin triplet and singlet states $|\pm\rangle=(|2\rangle\pm|1\rangle)/\sqrt{2}$ obtained by diagonalizing Eq. (2). They are separated in energy by $2J_{\rm ex}$, featuring the superexchange-driven evolution. Under the unitary transformation, inter-orbital spin-exchange-mediated coupling ($|1\rangle\leftrightarrow|3\rangle$) is equivalent to two couplings $|3\rangle\leftrightarrow|\pm\rangle$ with the strengths $\Omega_{1,2}=\mp V_{\rm ex}/\sqrt{2}$ in the new basis. Up to now, the problem is illustrated as a three-level system in Fig. 1(c). For $V_{\rm ex}\ll J_{\rm ex}$, the state $|3\rangle$ is far-off-resonant to the lowest state $|-\rangle$ and is near-resonant to the state $|+\rangle$. Ignoring the far-off-resonant coupling and only keeping the near-resonant coupling (Ω_1), we can easily obtain the final eigenstates ($|a\rangle,|b\rangle,|c\rangle$) (See Appendices for details). Consequently, the dynamical evolution N_{gz} contains two frequencies corresponding to the energy gaps $E_{\rm c}-E_{\rm a}$ and $E_{rmb}-E_{\rm a}$, respectively. Finally we extract analytic expression of the envelope as $\sqrt{5+4\cos(3V_{\rm ex}t/2)}/3$ (red solid in Fig. 1(b)). In this case, $h_{\rm c}=2/3$, $t_{\rm c}=2\pi/(3V_{\rm ex})$ and $t_{\rm r}=2t_{\rm c}$.

The results are in good agreement with the numerical solution of the full Hamiltonian Eq. (1), which indicates the validity of our perturbation treatment presented here. In particular, for $\Delta_B = V_{ex}/4$, $|3\rangle$ and $|+\rangle$ are degenerate in energy. We immediately arrive at an interesting phenomenon that the superexchange oscillation is totally suppressed and then restored as shown in Fig. 1(d). To obtain the requirement, one can increase the magnetic field or tune V_{ex} by adjusting the overlap of the g and e atomic wavepackets. In this situation $N_{gz}(t)$ shows an oscillating profile and the amplitude varies from one to zero periodically. N_{gz} vanishes till $t_c = \pi/(\sqrt{2}V_{ex})$ and subsequently restores gradually to its maximum at $t_r = 2t_c$. The exact derivations are given in Appendix B. The above analysis shows that the fast oscillation of the Néel order parameter still reflects the superexchange-dominating spin dynamics, and the slowly changing envelope originates from the coherent process between the magnetic and non-magnetic states caused by the local spin-exchange interaction. So far, we have given a clear physical picture to explain the modulated magnetization dynamics when the half-filling magnetic impurity occurs in the AFM ordered system.

4. Effect of the localized atom filling

In the aforementioned discussions, we have shown that the appearance of a single impurity atom indeed leads to significant modulation of the amplitude of the g atom spin dynamics in the double-well potential. Next we will explore the effect of the filling of the e atoms on the superexchange-mediated quantum magnetism. As shown in Fig. 2(a), the spin-polarized e atoms are deeply located in both wells. Similarly, we first numerically solve the full Hamiltonian to obtain N_{gz} as shown in Fig. 2(b). For comparison, the envelopes of the time-resolved spin dynamics at unit- and half-filling cases are depicted by the red solid curve and the blue dashed curve, respectively. They have a distinct feature that the amplitude of the antiferromagnetic exchange is periodically varied. Moreover, in comparison with the doping impurity at half-filling case, the modulated spin dynamics seems to be accelerated. In fact, the periodicity of the amplitude envelop decreases, which is consistent with smaller t_c and t_r. To illustrate the effect of the impurity filling, we adopt the same steps in the analysis of Fig. 1. Starting with the schematic diagram Fig. 2(a), after adiabatically eliminating the double occupancy and transforming the system into the basis composed of the spin singlet/spin triplet states $|\pm\rangle$, we have a symmetric level diagram as shown in Fig. 2(c). It is not surprising since the spin-exchange interaction can happen in both subwells and there are two coupling paths between the antiferromagnetic and non-magnetic states with the strength $-V_{ex}$. These couplings in the real process contribute all the transitions labeled by $\Omega_{1,2}$. Following the routine analysis on the half-filling situation, we need to perform the perturbation calculations in the low-energy subspace including the relevant states. In Fig. 2(c), the two magnetic states and the $|+\rangle$ state form a degenerate manifold that are resonantly coupled and separated with the $|-\rangle$ state by $2J_{ex}$. Since the coupling strengths are the same in magnitude, the lowest state $|-\rangle$ is just slightly shifted by off-resonant coupling from states $|3\rangle$ and $|4\rangle$. We can then obtain the eigenstates $|a\rangle$, $|b\rangle$, $|c\rangle$, and $|d\rangle$. As a direct consequence, the state $|c\rangle = (|4\rangle - |3\rangle)/2$ is orthogonal to the initial state $|1\rangle$, which means $|c\rangle$ should not be populated during the evolution. Finally, the dynamical evolution of the spin imbalance still contains two frequencies $E_{b,d} - E_a$, i.e.,

$$N_{gz}(t) \simeq \frac{1}{2}[\cos((2J_{ex} - V_{ex})t) + \cos((2J_{ex} + V_{ex})t)]$$

(for example, see Appendices for details). Apparently, the amplitude of the superexchange evolution is modulated with the frequency V_{ex}, which is $\sqrt{2}$ times that of the half-filling case and clearly reflects the influence of the local spin-exchange interaction. It also shows that the filling of the localized atoms plays a significant role in temporally manipulating the magnetism even in the superexchange-dominating limit.

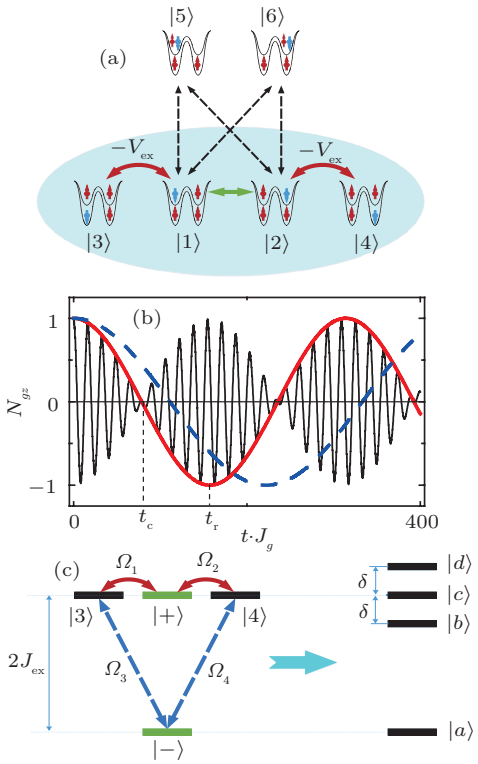


Fig. 2. (color online) (a) Schematic diagram of the superexchange and inter-orbital spin-exchange interactions at unit-filling of the e atoms. (b) Time evolution of spin imbalance N_{gz} (black solid). The envelopes of $N_{gz}(t)$ at unit-filling (red solid) and half-filling (blue dashed) have been shown. t_c and t_r are the collapse and revival periods, respectively. The parameters are $U_{gg} = 10J_g$, $V = 0.025J_g$, $V_{ex} = 0.02J_g$. The envelope (red solid) is $\cos(V_{ex}t)$. The collapse and revival happen at t_c and t_r, respectively. (c) Energy levels in the low-energy effective Hamiltonian (left) and the eigenstates (right). $|\pm\rangle = (|2\rangle \pm |1\rangle)/\sqrt{2}$. $\Omega_1 = \Omega_2 = \Omega_4 = -V_{ex}/\sqrt{2}$ and $\Omega_3 = V_{ex}/\sqrt{2}$ are the coupling matrix elements. $\delta = V_{ex}$ is the energy shift. The red solid and blue dashed arrows indicate the near-resonant and far-off-resonant couplings, respectively.

5. Experimental accessibility

Now we turn to discuss experimental requirements for observing the amplitude-varying superexchange-dominating magnetization dynamics. It is requisite to prepare the initial state with the AFM order of the g atoms and one e atom. First, we have to prepare a spin mixture with two $g\uparrow$ atoms and one $g\downarrow$ in the long lattice, which can be realized by carefully tuning the state transfer from $|\uparrow_g\rangle$ to $|\downarrow_g\rangle$ in a spin-polarized Fermi gas. Then we load a band insulator with $|\uparrow_g\downarrow_g\rangle$ atoms in the ground band and one $|\uparrow_g\rangle$ in the first excited band per site on the deep long lattice. Subsequently we ramp up the short lattice with a bias to build a double-well array that it is energetically favorable to have two atoms with different spins in the left well and one atom in the right well. Finally we perform a π-polarized clock excitation solely resonant with the $|\uparrow_g\rangle_{\rm L}\rightarrow|\uparrow_e\rangle_{\rm L}$ transition that is off-resonant for $|\downarrow_g\rangle_{\rm L}\rightarrow|\downarrow_e\rangle_{\rm L}$ when the differential Zeeman shift $\Delta_{\rm B}$ is larger than the linewidth of the clock excitation. In addition, the single-occupied site can be spectroscopically resolved due to large U_{gg}. To measure N_{gz}, we release the e atoms in the lattice by transferring them to the $^3{\rm S}_1$ state, and subsequently band mapping technique is used to extract the information of the g atoms. These can be reached within the-state-of-the-art experimental efforts. The initial state in Fig. 2 can also be prepared with the similar strategy. Moreover, the spin-exchange interaction is expected to be tuned by the recently proposed orbital Feshbach resonance technique,[33] which has been experimentally demonstrated with ultracold ^{173}Yb atoms.[34,35]

6. Conclusion

In conclusion, we have theoretically studied the superexchange-mediated magnetization dynamics with ultracold AEAs in an optical superlattice. We found that, the doped $^3{\rm P}_0$ atoms and the associated spin-exchange interaction between the clock states give rise to the modulation superexchange dynamics, especially when the superexchange interaction predominates in the system. As a particular example, the appearance of the modulating oscillation in the magnetization dynamics has shown the doped magnetic impurities indeed play an important role in the superexchange interaction by coherent spin-exchange mechanism. We have also found that, compared to the half-filling case of the e atom, the modulated spin dynamics of the g atoms can indeed be accelerated at unit-filling. Our findings may provide new insights in coherent control of quantum magnetism with hidden symmetric intrinsic interactions between ultracold atoms.

Appendix A: Perturbation method

For clarify, we start with the terminology for the dynamics of the atoms in the optical lattice. Generally, we use the term 'coupling' to represent the transition between atomic states before and after the tunneling and the inter-atomic interactions. In this sense, the coupling can happen during the tunneling process like $|\uparrow_g,\downarrow_g\rangle\rightarrow|0,\uparrow_g\downarrow_g\rangle$ or the spin-exchange interaction like $|\uparrow_g\downarrow_e,0\rangle\rightarrow|\downarrow_g\uparrow_e,0\rangle$. Without generality, as sketched in Fig. S1(a), the simplest coupling between the two quantum states can be described by the Hamiltonian

$$\hat{H}=\frac{\Delta}{2}(|2\rangle\langle 2|-|1\rangle\langle 1|)+\Omega_0(|2\rangle\langle 1|+|1\rangle\langle 2|),$$

where Δ is energy difference and Ω_0 is coupling strength (see Fig. S1). The resulting eigenstates are

$$|\pm\rangle\propto\frac{-\Delta\pm\Omega}{2\Omega_0}|1\rangle+|2\rangle, \tag{A1}$$

with the eigenenergies $E_\pm=\pm\Omega/2$ and $\Omega=\sqrt{4\Omega_0^2+\Delta^2}$. The eigenstates $|\pm\rangle$ have the energy shifts $\pm\delta_0$ from the bare states. For $|\Delta|\gg|\Omega_0|$ (far-off-resonance), $\delta_0\sim\Omega_0^2/|\Delta|$ is very small. However, when the coupling strength $|\Omega_0|$ is comparable to or even much greater than $|\Delta|$, the coupling becomes near-resonant. In particular, for the coupling between degenerate states with $\Delta=0$, we have $\Omega=2|\Omega_0|$. We are interested in the change of the population difference of the two-level system, i.e., $N_z(t)=P_1(t)-P_2(t)$, where $P_{1,2}$ are the populations of the two states. It is easy to obtain

$$N_z(t)=\frac{\Delta^2+4\Omega_0^2\cos(\Omega t)}{\Omega^2}. \tag{A2}$$

For $\Delta=0$, it arrives at an oscillation at the frequency $2\Omega_0$. One can observe the oscillating behavior in Eq. (A2) to identify the coupling.

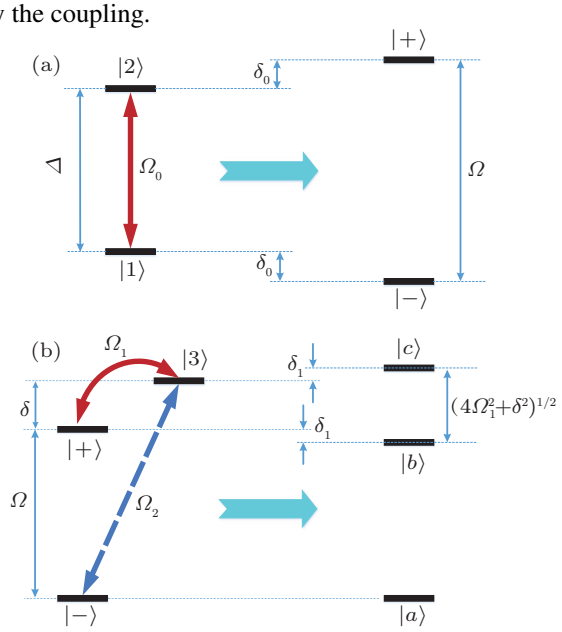


Fig. S1. (color online) (a) Schematic diagram of the coupling between the two quantum states (left) and energy levels of the eigenstates (right). Δ and Ω_0 are the energy difference and coupling strength, respectively. Ω is the energy difference between the two eigenstates. δ_0 is the energy shift. (b) The three-level model for strong (Ω) and weak ($\Omega_{1,2}$) couplings in perturbation theory (left) and energy eigenstates (right). δ and δ_1 are the energy difference and the energy shift. The red solid (blue dashed) arrow labels the near-resonant (far-off-resonant) coupling.

Consider the situation that the two-level system is perturbed by another weak coupling that only gives rise to the transition between $|1\rangle$ and an auxiliary state $|3\rangle$. As shown in Fig. S1(b), the weak coupling is now equivalent to the couplings between $|\pm\rangle$ and $|3\rangle$ with the respective strengths $|\Omega_{1,2}| \ll |\Omega_0|$. Given that $|\Omega_2| \ll |\Omega+\delta|$ and Ω_1 is comparable to δ, the $|3\rangle \leftrightarrow |+\rangle$ coupling is near-resonant while the $|3\rangle \leftrightarrow |-\rangle$ coupling becomes far-off-resonant. Now we adopt a trick to obtain the eigenstates of the total system analytically. We ignore the far-off-resonant coupling and only consider the influence of the near-resonant coupling on the energy levels. Consequently, we write the eigenstates and eigenenergies explicitly as follows:

$$\begin{aligned}
&|a\rangle \propto |-\rangle, \ \ E_a \simeq -\frac{\Omega}{2},\\
&|b\rangle \propto \frac{-\delta-\sqrt{\delta^2+4\Omega_1^2}}{2\Omega_1}|+\rangle+|3\rangle,\\
&E_b \simeq \frac{\Omega+\delta}{2}-\sqrt{\left(\frac{\delta}{2}\right)^2+\Omega_1^2},\\
&|c\rangle \propto \frac{-\delta+\sqrt{\delta^2+4\Omega_1^2}}{2\Omega_1}|+\rangle+|3\rangle,\\
&E_c \simeq \frac{\Omega+\delta}{2}+\sqrt{\left(\frac{\delta}{2}\right)^2+\Omega_1^2}.
\end{aligned} \tag{A3}$$

In this case, starting with the initial state $|1\rangle$, the resulting population difference $N_z(t)$ comprises several oscillation components, the angular frequencies of which are the energy differences between pairs of the eigenstates ($|a\rangle$, $|b\rangle$ and $|c\rangle$). Further, when the condition $|\Delta| \ll |\Omega_0|$ is satisfied, $N_z(t)$ comprises two oscillation components with the frequencies $E_c - E_a$ and $E_b - E_a$ and can be expressed by

$$N_z(t) = A_1 \cos[(\Omega+\Delta_1)t] + A_2 \cos[(\Omega+\Delta_2)t], \tag{A4}$$

where $A_{1,2}$ correspond to the oscillation amplitudes, and

$$\Delta_{1,2} = \delta/2 \mp \sqrt{(\delta/2)^2+\Omega_1^2}$$

are the shifts relative to the oscillation frequency without the weak coupling. We further write the above equation into the form $N_z(t) = A_m(t)\cos[\Omega t + \varphi_m(t)]$ with amplitude-modulation factor

$$A_m(t) = \sqrt{A_1^2+A_2^2+2A_1A_2\cos[(\Delta_1-\Delta_2)t]}.$$

After an interval $t_c = \pi/|\Delta_1-\Delta_2|$, A_m reaches the minimum and restores back at $t_r = 2t_c$.

When the two oscillation components have the same weight ($A_1 = A_2 = 1/2$),

$$N_z(t) = \cos\left(\frac{\Delta_1-\Delta_2}{2}t\right)\cos\left[\left(\Omega+\frac{\Delta_1+\Delta_2}{2}\right)t\right], \tag{A5}$$

representing an oscillation at frequency $\Omega+(\Delta_1+\Delta_2)/2$ whose amplitude is modulated by a slow oscillation at frequency $|\Delta_1-\Delta_2|/2$. For the scenario in Fig. S1(b), when the weak coupling between $|+\rangle$ and $|3\rangle$ is totally resonant ($\delta = 0$), the condition $A_1 = A_2 = 1/2$ can be satisfied and the population difference is reduced to

$$N_z(t) = \cos(\Omega_1 t)\cos(\Omega t). \tag{A6}$$

Appendix B: Superexchange dynamics at half-filling of the *e* atoms

We give the details on perturbation treatment of the superexchange process at half-filling of the localized atoms in the optical superlattices (see Fig. 1 in the main text). We first write the full Hamiltonian in the state basis with $\{|1\rangle,|2\rangle,|3\rangle,|4\rangle,|5\rangle\}$

$$\hat{H}_{\rm I} = \begin{pmatrix}
0 & 0 & -V_{\rm ex} & J_g & J_g\\
0 & -V_{\rm ex} & 0 & -J_g & -J_g\\
-V_{\rm ex} & 0 & -2\Delta_B & 0 & 0\\
J_g & -J_g & 0 & U_{gg}+V-V_{\rm ex} & 0\\
J_g & -J_g & 0 & 0 & U_{gg}-V
\end{pmatrix}. \tag{B1}$$

Here we have chosen the energy of the state $|1\rangle$ as the zero of energy. After eliminating the double-occupied states, we obtain the low-energy effective Hamiltonian in the subspace of $\{|1\rangle,|2\rangle,|3\rangle\}$ as follows:

$$\hat{H}_{\rm I}^{\rm eff} = \begin{pmatrix}
-J_{\rm ex} & J_{\rm ex} & -V_{\rm ex}\\
J_{\rm ex} & -J_{\rm ex}-V_{\rm ex} & 0\\
-V_{\rm ex} & 0 & -2\Delta_B
\end{pmatrix}. \tag{B2}$$

For $J_{\rm ex} \gg V_{\rm ex}$, the energy gap between the states ($|\pm\rangle$) obtained from diagonalizing the superexchange term is

$$\Omega = \sqrt{4J_{\rm ex}^2+V_{\rm ex}^2} \simeq 2J_{\rm ex}.$$

For AEAs, the differential Zeeman shift Δ_B at a low magnetic field can be negligible in the present situation. The effective Hamiltonian Eq. (B2) may be readily diagonalized, leading to the eigenstates and corresponding eigenenergies

$$\begin{aligned}
&|a\rangle = \frac{-|1\rangle+|2\rangle}{\sqrt{2}}, \ \ E_a = -2J_{\rm ex}-\frac{V_{\rm ex}}{2},\\
&|b\rangle = \frac{|1\rangle+|2\rangle+|3\rangle}{\sqrt{3}}, \ \ E_b = -V_{\rm ex},\\
&|c\rangle = \frac{-|1\rangle-|2\rangle+2|3\rangle}{\sqrt{6}}, \ \ E_c = \frac{V_{\rm ex}}{2},
\end{aligned} \tag{B3}$$

where higher-order terms have been omitted. Based on the analysis in Appendix A, after initially preparing the system in $|1\rangle$, we have

$$\begin{aligned}
N_{gz}(t) &= \frac{2}{3}\cos\left[\left(2J_{\rm ex}-\frac{V_{\rm ex}}{2}\right)t\right]+\frac{1}{3}\cos[(2J_{\rm ex}+V_{\rm ex})t]\\
&= A_m(t)\cos(2J_{\rm ex}t+\varphi_m),
\end{aligned} \tag{B4}$$

with

$$A_m(t) = \frac{1}{3}\sqrt{5+4\cos\left(\frac{3}{2}V_{\rm ex}t\right)}. \quad \text{(B5)}$$

When $\Delta_{\rm B} = V_{\rm ex}/4$, we have

$$|a\rangle = \frac{-|1\rangle+|2\rangle}{\sqrt{2}}, \ E_a = -2J_{\rm ex} - \frac{V_{\rm ex}}{2},$$

$$|b\rangle = \frac{|1\rangle+|2\rangle+\sqrt{2}|3\rangle}{2}, \ E_b = \frac{-1-\sqrt{2}}{2}V_{\rm ex}, \quad \text{(B6)}$$

$$|c\rangle = \frac{-|1\rangle-|2\rangle+\sqrt{2}|3\rangle}{2}, \ E_c = \frac{-1+\sqrt{2}}{2}V_{\rm ex}. \quad \text{(B7)}$$

As a result, the Néel order parameter is given by

$$N_{gz}(t) = \frac{1}{2}\cos\left[(2J_{\rm ex} - \frac{V_{\rm ex}}{\sqrt{2}})t\right] + \frac{1}{2}\cos\left[(2J_{\rm ex} + \frac{V_{\rm ex}}{\sqrt{2}})t\right]. \quad \text{(B8)}$$

One can immediately obtain the amplitude modulation as follows:

$$A_m(t) = \cos(V_{\rm ex}t/\sqrt{2}).$$

Appendix C: Superexchange dynamics at unit-filling of the spin-polarized *e* atoms

When the two e atoms are fixed in both subwells, following the analysis above, we explicitly write the total Hamiltonian in the basis of $\{|1\rangle,|2\rangle,|3\rangle,|4\rangle,|5\rangle,|6\rangle\}$

$$\hat{H}_{\rm II} = \begin{pmatrix} 0 & 0 & -V_{\rm ex} & 0 & J_g & J_g \\ 0 & 0 & 0 & -V_{\rm ex} & -J_g & -J_g \\ -V_{\rm ex} & 0 & 0 & 0 & 0 & 0 \\ 0 & -V_{\rm ex} & 0 & 0 & 0 & 0 \\ J_g & -J_g & 0 & 0 & U_{gg} & 0 \\ J_g & -J_g & 0 & 0 & 0 & U_{gg} \end{pmatrix}. \quad \text{(C1)}$$

Next, adiabatically eliminating $|5\rangle,|6\rangle$, we arrive at the effective Hamiltonian in the subspace of $\{|1\rangle,|2\rangle,|3\rangle,|4\rangle\}$

$$\hat{H}_{\rm II}^{\rm eff} = \begin{pmatrix} -J_{\rm ex} & J_{\rm ex} & -V_{\rm ex} & 0 \\ J_{\rm ex} & -J_{\rm ex} & 0 & -V_{\rm ex} \\ -V_{\rm ex} & 0 & 0 & 0 \\ 0 & -V_{\rm ex} & 0 & 0 \end{pmatrix}. \quad \text{(C2)}$$

The energy eigenstates and the corresponding eigenvalues are

$$|a\rangle = \frac{-|1\rangle+|2\rangle}{\sqrt{2}}, \ E_a = -2J_{\rm ex},$$

$$|b\rangle = \frac{|1\rangle+|2\rangle+|3\rangle+|4\rangle}{2}, \ E_b = -V_{\rm ex},$$

$$|c\rangle = \frac{-|3\rangle+|4\rangle}{\sqrt{2}}, \ E_c = 0,$$

$$|d\rangle = \frac{-|1\rangle-|2\rangle+|3\rangle+|4\rangle}{2}, \ E_d = V_{\rm ex}. \quad \text{(C3)}$$

Finally, the spin imbalance can be easily obtained

$$N_{gz}(t) = \frac{1}{2}\cos[(2J_{\rm ex}-V_{\rm ex})t] + \frac{1}{2}\cos[(2J_{\rm ex}+V_{\rm ex})t] \quad \text{(C4)}$$

with the amplitude modulation factor $A_m(t) = \cos(V_{\rm ex}t)$.

References

[1] Bloch I, Dalibard J, and Zwerger W 2008 *Rev. Mod. Phys.* **80** 885

[2] Lewenstein M, Sanpera A and Ahufinger V 2012 *Ultracold atoms in optical lattices: simulating quantum many-body systems* (Oxford: Oxford University Press), ISBN: 0199573123

[3] Bloch I, Dalibard J and Nascimbene S 2012 *Nat. Phys.* **8** 267

[4] Jaksch D, Bruder C, Cirac J I, Gardiner C W and Zoller P 1998 *Phys. Rev. Lett.* **81** 3108

[5] Greiner M, Mandel O, Esslinger T, Hänsch T W and Bloch I 2002 *Nature* **415** 39

[6] Jaksch D and Zoller P 2005 *Ann. Phys.* **315** 52

[7] Jördens R, Strohmaier N, Günther K, Moritz H and Esslinger T 2008 *Nature* **455** 204

[8] Schneider U, Hackermüller L, Will S, Best T, Bloch I, Costi T A, Helmes R W, Rasch D and Rosch A 2008 *Science* **322** 1520

[9] Esslinger T 2010 *Ann. Rev. Condens. Matter Phys.* **1** 129

[10] Duan L M, Demler E and Lukin M D 2003 *Phys. Rev. Lett.* **91** 090402

[11] Kuklov A B and Svistunov B V 2003 *Phys. Rev. Lett.* **90** 100401

[12] Altman E, Hofstetter W, Demler E and Lukin M D 2003 *New J. Phys.* **5** 113

[13] Mandel O, Greiner M, Widera A, Rom T, Hansch T W and Bloch I 2003 *Nature* **425** 937

[14] Anderlini M, Lee P J, Brown B L, Sebby-Strabley J, Phillips W D and Porto J V 2007 *Nature* **448** 452

[15] Kaufman A M, Lester B J, Foss-Feig M, Wall M L, Rey A M and Regal C A 2015 *Nature* **527** 208

[16] Yan B, Moses S A, Gadway B, Covey J P, Hazzard K R A, Rey A M, Jin D S and Ye J 2013 *Nature* **501** 521

[17] Rey A M, Gritsev V, Bloch I, Demler E and Lukin M D 2007 *Phys. Rev. Lett.* **99** 140601

[18] Trotzky S, Cheinet P, Fölling S, Feld M, Schnorrberger U, Rey A M, Polkovnikov A, Demler E A, Lukin M D and Bloch I 2008 *Science* **319** 295

[19] Chen Y A, Nascimbene S, Aidelsburger M, Atala M, Trotzky S and Bloch I 2011 *Phys. Rev. Lett.* **107** 210405

[20] Brown R C, Wyllie R, Koller S B, Goldschmidt E A, Foss-Feig M and Porto J V 2015 *Science* **348** 540

[21] Gorshkov A V, Hermele M, Gurarie V, Xu C, Julienne P S, Ye J, Zoller P, Demler E, Lukin M D and Rey A M 2010 *Nat. Phys.* **6** 289

[22] Cazalilla M A and Rey A M 2014 *Rep. Prog. Phys.* **77**

[23] Zhang X, Bishof M, Bromley S L, Kraus C V, Safronova M S, Zoller P, Rey A M and Ye J 2014 *Science* **345** 1467

[24] Scazza F, Höfrichter C, Hofer M, De Groot P C, Bloch I and Fölling S 2014 *Nat. Phys.* **10** 779

[25] Cappellini G, Mancini M, Pagano G, Lombardi P, Livi L, de Cumis M S, Cancio P, Pizzocaro M, Calonico D, Levi F, Sias C, Catani J, Inguscio M and Fallani L 2014 *Phys. Rev. Lett.* **113** 120402

[26] Hewson A C 1993 *The Kondo problem to heavy fermions* (Cambridge: Cambridge University Press), ISBN: 0521363829

[27] Coleman P 2015 *Introduction to many-body physics* (Cambridge: Cambridge University Press) Chap. 16–17, ISBN: 0521864887

[28] Foss-Feig M, Hermele M and Rey A M 2010 *Phys. Rev. A* **82** 053624

[29] Hazzard K R A, Gurarie V, Hermele M and Rey A M 2012 *Phys. Rev. A* **85** 041604

[30] Hofrichter C, Riegger L, Scazza F, Höfer M, Fernandes D R, Bloch I and Fölling S 2016 *Phys. Rev. X* **6** 021030

[31] Auerbach A 1994 *Interacting electrons and quantum magnetism* (New York: Springer-Verlag) pp. 16–18, ISBN: 0387942866

[32] Boyd M M, Zelevinsky T, Ludlow A D, Blatt S, Zanon-Willette T, Foreman S M and Ye J 2007 *Phys. Rev. A* **76** 022510

[33] Zhang R, Cheng Y T, Zhai H and Zhang P 2015 *Phys. Rev. Lett.* **115** 135301

[34] Pagano G, Mancini M, Cappellini G, Livi L, Sias C, Catani J, Inguscio M and Fallani L 2015 *Phys. Rev. Lett.* **115** 265301

[35] Höfer M, Riegger L, Scazza F, Hofrichter C, Fernandes D R, Parish M M, Levinsen J, Bloch I and Fölling S 2015 *Phys. Rev. Lett.* **115** 265302